optica

Dynamic suppression of Rayleigh backscattering in dielectric resonators: supplementary material

SEUNGHWI KIM[1], JACOB M. TAYLOR[2,3], AND GAURAV BAHL[1,*]

[1]Mechanical Science and Engineering, University of Illinois at Urbana-Champaign, Urbana, Illinois 61801, USA
[2]Joint Quantum Institute, University of Maryland, College Park, Maryland 20742, USA
[3]National Institute of Standards and Technology, Gaithersburg, Maryland 20899, USA
[*]Corresponding author: bahl@illinois.edu

Published 7 August 2019

This document provides supplementary information to "Dynamic suppression of Rayleigh backscattering in dielectric resonators," https://doi.org/10.1364/OPTICA.6.001016.

1. SYSTEM MODEL INCLUDING RAYLEIGH SCATTERING AND OPTOMECHANICAL COUPLING

Our whispering gallery resonator (WGR) system supports two frequency-adjacent optical modes, the mode of interest $a_\pm$ and Stokes shifted pump mode $c_\pm$, and a mechanical mode $b_\pm$. All three modes are of whispering gallery mode (WGM) type and exist as degenerate pairs in the cw (+) and ccw (-) direction. As described in the main text (Fig. 1), the cw optical modes a_+ and c_+ couple through the cw mechanical mode b_+ via optomechanical interaction:

$$H_{\text{int}}^{\text{OM}} = \hbar(g_o c_+ a_+^\dagger b_+ + g_o^* c_+^\dagger a_+ b_+^\dagger)$$

We define the single photon Brillouin optomechanical coupling rate $g_o \propto \delta(\Delta k) \int \phi_1 \phi_2 \psi \, d^2r$, where ϕ_1, ϕ_2 and ψ are the transverse mode shapes of the optical and mechanical modes, respectively. The delta function $\delta(\Delta k)$ represents the momentum selection condition for Brillouin scattering, i.e. the momentum difference between the optical modes a_+ and c_+ must match the momentum of the mechanical mode b_+. We also consider the interaction of the cw optical modes (a_+, c_+) with their time-reversed counterparts (a_-, c_-) via elastic Rayleigh backscattering. This coupling can be induced by surface or internal inhomogeneities [1–4] in WGRs. Under the dipole approximation, we can write the interaction Hamiltonian due to Rayleigh scattering for the optical mode pairs as follows [5]:

$$H_{\text{int}}^{\text{R}} = \hbar V_o (a_+^\dagger a_- + a_-^\dagger a_+) + \hbar V_1 (c_+^\dagger c_- + c_-^\dagger c_+)$$

Here, we have defined V_o and V_1 as the backscattering rates for the $a_\pm$ and $c_\pm$ modes, respectively. These coupling rates are given by $2V_{i=0,1} = -\alpha f_i^2(r)\omega_i/\mathcal{V}_{\text{m}}^i$ where α is the polarizability of the scatterer, $f_i(r)$ accounts for the overlap of the optical field with the scatterer dipole, ω_i is the resonant frequency of the optical mode and $\mathcal{V}_{\text{m}}^i$ is its modal volume [5]. The normal-mode splitting induced by Rayleigh backscattering is easily experimentally observable if $V_i > \kappa/2$.

Considering the two interaction Hamiltonians, we can now represent the linearized Heisenberg-Langevin equations of our system. Under the non-depleted pump approximation we are able to omit the equations for $c_\pm$, which leads to the equations of motion:

$$\begin{aligned} \frac{da_+}{dt} &= -\left(\frac{\kappa}{2} + i\Delta_a\right) a_+ - iGb_+ - iV_o a_- + \sqrt{\kappa_{\text{ex}}} a_+^{\text{in}}(t) \\ &\quad + \sqrt{\kappa_i} a_{\text{vac}}(t), && \text{(S1a)} \\ \frac{db_+}{dt} &= -\left(\frac{\Gamma}{2} + i\Delta_b\right) b_+ - iG^* a_+ + \sqrt{\Gamma} b_{\text{th}}(t), && \text{(S1b)} \\ \frac{da_-}{dt} &= -\left(\frac{\kappa}{2} + i\Delta_a\right) a_- - \eta G b_- - iV_o a_+ + \sqrt{\kappa_{\text{ex}}} a_-^{\text{in}}(t) \\ &\quad + \sqrt{\kappa_i} a_{\text{vac}}(t), && \text{(S1c)} \\ \frac{db_-}{dt} &= -\left(\frac{\Gamma}{2} + i\Delta_b\right) b_- + \eta G^* a_- + \sqrt{\Gamma} b_{\text{th}}(t). && \text{(S1d)} \end{aligned}$$

Here $a_\pm^{\text{in}}$ are the normalized probe laser amplitudes within the waveguide, in forward (+) and backward (-) directions. They are defined as $|a_\pm^{\text{in}}|^2 = P_{\text{probe}\pm}^{\text{in}}/\hbar\omega_{\text{probe}}$, where $P_{\text{probe}\pm}^{\text{in}}$ is the corresponding input probe laser power into the waveguide and ω_{probe} is the probe laser frequency. $\sqrt{\kappa_{\text{ex}}}$ appears due to the external coupling to a side-coupled waveguide. $a_{\text{vac}}(t)$ and $b_{\text{th}}(t)$ are the vacuum and thermal noise in the optical and mechanical modes, respectively. κ and Γ are the total loss rates of the $a_\pm$ and $b_\pm$ modes respectively. The detuning terms are defined as $\Delta_a = \omega_a - \omega_{\text{probe}}$ and $\Delta_b = \omega_b - (\omega_{\text{probe}} - \omega_{\text{pump}})$, where ω_a and ω_b are resonant frequencies of $a_\pm$ and $b_\pm$ modes respectively, and ω_{pump} is the pump laser frequency. $G \triangleq g_o\sqrt{n_p}$ is the pump-enhanced optomechanical coupling due to the c_+ pump. Since we also wish to take into account Rayleigh scattering for the $c_\pm$ modes, there may be some backscattered pump power from the cw pump mode c_+ into the ccw pump mode c_-, which creates non-zero optomechanical interaction in the ccw direction. In the above equations we have incorporated this ccw optomechanical interaction by introducing $\eta = 2V_1/\kappa_c$, where κ_c is the optical loss rate of the $c_\pm$ modes. After this accounting we are no longer interested in the pump equations of motion, so we can dispense with the $V_{0,1}$ distinctions and instead replace a single backscattering rate $V = V_0$ between the $a_\pm$ modes.

Fig. S1 presents the toy model of our system, in which the forward and backward subsystems of the resonator are deliberately identified separately. As explained in the main text, the transmission coefficients must be different (Fig. S1b and S1c). On the other hand, the two reflection coefficients must be identical since the light experiences both forward and backward optical susceptibilities in series (Fig. S1d and S1e), i.e. the reflection system is identical in either direction ($R = R_{11} = R_{22}$).

A. Waveguide transmission and reflection coefficients

To experimentally investigate the optomechanical modification of Rayleigh backscattering within the resonator, we can perform measurements of the transmission and reflection coefficients through the side-coupled waveguide. Since we are interested in the stationary solutions of Eqns. S1, we can neglect the vacuum and thermal noise in our calculation. The steady state intracavity field solutions $\bar{a}_+$ and $\bar{a}_-$ excited by both forward and backward probe fields are obtained as follows :

$$\bar{a}_+ = \frac{\sqrt{\kappa_{\text{ex}}}a_+^{\text{in}} - \dfrac{iV(\Gamma/2+i\Delta_b)\sqrt{\kappa_{\text{ex}}}a_-^{\text{in}}}{(\kappa/2+i\Delta_a)(\Gamma/2+i\Delta_b)+\eta^2G^2}}{\dfrac{\kappa}{2}+i\Delta_a+\dfrac{G^2}{\Gamma/2+i\Delta_b}+\dfrac{V^2(\Gamma/2+i\Delta_b)}{(\kappa/2+i\Delta_a)(\Gamma/2+i\Delta_b)+\eta^2G^2}}, \tag{S2a}$$

$$\bar{a}_- = \frac{\sqrt{\kappa_{\text{ex}}}a_-^{\text{in}} - \dfrac{iV(\Gamma/2+i\Delta_b)\sqrt{\kappa_{\text{ex}}}a_+^{\text{in}}}{(\kappa/2+i\Delta_a)(\Gamma/2+i\Delta_b)+G^2}}{\dfrac{\kappa}{2}+i\Delta_a+\dfrac{\eta^2G^2}{\Gamma/2+i\Delta_b}+\dfrac{V^2(\Gamma/2+i\Delta_b)}{(\kappa/2+i\Delta_a)(\Gamma/2+i\Delta_b)+G^2}}. \tag{S2b}$$

The above expressions show that the cavity modes can be populated by both forward and backward optical probes, due to the Rayleigh backscattering. Using the resonator input-output formalism, we now can obtain expressions for the output fields in the waveguide (Fig. S2).

1. for cw transmission $a_+^{\text{out}}|_{a_-^{\text{in}}=0} = a_+^{\text{in}} - \sqrt{\kappa_{\text{ex}}}\,\bar{a}_+|_{a_-^{\text{in}}=0}$
2. for ccw transmission $a_-^{\text{out}}|_{a_+^{\text{in}}=0} = a_-^{\text{in}} - \sqrt{\kappa_{\text{ex}}}\,\bar{a}_-|_{a_+^{\text{in}}=0}$
3. for cw $\rightarrow$ ccw reflection $a_-^{\text{out}}|_{a_-^{\text{in}}=0} = -\sqrt{\kappa_{\text{ex}}}\,\bar{a}_-|_{a_-^{\text{in}}=0}$
4. for ccw $\rightarrow$ cw reflection $a_+^{\text{out}}|_{a_+^{\text{in}}=0} = -\sqrt{\kappa_{\text{ex}}}\,\bar{a}_+|_{a_+^{\text{in}}=0}$

The above expressions allow us to derive the waveguide transmission and reflection coefficients as follows :

$$\begin{aligned} T_{21} &= \left.\frac{a_+^{\text{out}}}{a_+^{\text{in}}}\right|_{a_-^{\text{in}}=0} \\ &= 1 - \frac{\kappa_{\text{ex}}}{\dfrac{\kappa}{2}+i\Delta_a+\dfrac{G^2}{\Gamma/2+i\Delta_b}+\dfrac{V^2(\Gamma/2+i\Delta_b)}{(\kappa/2+i\Delta_a)(\Gamma/2+i\Delta_b)+\eta^2G^2}}, \end{aligned} \tag{S3a}$$

$$\begin{aligned} T_{12} &= \left.\frac{a_-^{\text{out}}}{a_-^{\text{in}}}\right|_{a_+^{\text{in}}=0} \\ &= 1 - \frac{\kappa_{\text{ex}}}{\dfrac{\kappa}{2}+i\Delta_a+\dfrac{V^2}{\kappa/2+i\Delta_a+G^2/(\Gamma/2+i\Delta_b)}+\dfrac{\eta^2G^2}{\Gamma/2+i\Delta_b}}, \end{aligned} \tag{S3b}$$

$$\begin{aligned} R &= \left.\frac{a_-^{\text{out}}}{a_+^{\text{in}}}\right|_{a_-^{\text{in}}=0} = \left.\frac{a_+^{\text{out}}}{a_-^{\text{in}}}\right|_{a_+^{\text{in}}=0} \\ &= \frac{\dfrac{iV\kappa_{\text{ex}}}{\kappa/2+i\Delta_a+G^2/(\Gamma/2+i\Delta_b)}}{\dfrac{\kappa}{2}+i\Delta_a+\dfrac{V^2}{\kappa/2+i\Delta_a+G^2/(\Gamma/2+i\Delta_b)}+\dfrac{\eta^2G^2}{\Gamma/2+i\Delta_b}}. \end{aligned} \tag{S3c}$$

We can also consider the case where there is no backscattering of the pump, i.e. $\eta = 0$, which results in the simplified equations :

$$T_{21} = \left.\frac{a_+^{\text{out}}}{a_+^{\text{in}}}\right|_{a_-^{\text{in}}=0} = 1 - \frac{\kappa_{\text{ex}}}{\dfrac{\kappa}{2}+i\Delta_a+\dfrac{G^2}{\Gamma/2+i\Delta_b}+\dfrac{V^2}{\kappa/2+i\Delta_a}} \tag{S4a}$$

$$T_{12} = \left.\frac{a_-^{\text{out}}}{a_-^{\text{in}}}\right|_{a_+^{\text{in}}=0} = 1 - \frac{\kappa_{\text{ex}}}{\dfrac{\kappa}{2}+i\Delta_a+\dfrac{V^2}{\kappa/2+i\Delta_a+G^2/(\Gamma/2+i\Delta_b)}} \tag{S4b}$$

$$\begin{aligned} R &= \left.\frac{a_-^{\text{out}}}{a_+^{\text{in}}}\right|_{a_-^{\text{in}}=0} = \left.\frac{a_+^{\text{out}}}{a_-^{\text{in}}}\right|_{a_+^{\text{in}}=0} \\ &= \frac{\dfrac{iV\kappa_{\text{ex}}}{\kappa/2+i\Delta_a+G^2/(\Gamma/2+i\Delta_b)}}{\dfrac{\kappa}{2}+i\Delta_a+\dfrac{V^2}{\kappa/2+i\Delta_a+G^2/(\Gamma/2+i\Delta_b)}} \end{aligned} \tag{S4c}$$

Finally, we can also produce a scattering matrix formalism for the the optical probe transmission and reflection coefficients, that incorporates simultaneous inputs from both directions in the waveguide:

$$\begin{pmatrix} a_-^{\text{out}} \\ a_+^{\text{out}} \end{pmatrix} = \begin{pmatrix} R_{11} & T_{12} \\ T_{21} & R_{22} \end{pmatrix} \begin{pmatrix} a_+^{\text{in}} \\ a_-^{\text{in}} \end{pmatrix} \tag{S5}$$

Here we see that the scattering matrix is generally non-symmetric, i.e. $T_{12} \neq T_{21}$, when the optomechanical coupling is non-zero. This non-reciprocity of transmission coefficients induced through Brillouin scattering has been already reported [6, 7].

B. Effective optical loss rate

Optical loss due to Rayleigh backscattering is typically included as a part of the intrinsic loss in whispering gallery resonators, since it cannot be distinguished from absorption losses at low scattering rates. In this work, however, we must explicitly distinguish the optical loss due to Rayleigh backscattering from other intrinsic optical losses. To quantify the optical loss, we first focus on the susceptibilities for the $a_\pm$ modes using Eqs. S1. Solving in the Fourier domain, we obtain

$$\begin{aligned}\chi_{a_+}^{-1}(\omega) &= -i(\omega-\Delta_a)+\kappa/2\\ &+\frac{G^2}{-i(\omega-\Delta_b)+\Gamma/2}\\ &+\frac{V^2(-i(\omega-\Delta_b)+\Gamma/2)}{(-i(\omega-\Delta_a)+\kappa/2)(-i(\omega-\Delta_b)+\Gamma/2)+\eta^2G^2}, \text{ and}\end{aligned} \tag{S6a}$$

$$\begin{aligned}\chi_{a_-}^{-1}(\omega) &= -i(\omega-\Delta_a)+\kappa/2\\ &+\frac{\eta^2G^2}{-i(\omega-\Delta_a)+\Gamma/2}\\ &+\frac{V^2\left(-i(\omega-\Delta_b)+\Gamma/2\right)}{\left(-i(\omega-\Delta_a)+\kappa/2\right)\left(-i(\omega-\Delta_b)+\Gamma/2\right)+G^2}.\end{aligned} \tag{S6b}$$

The effective optical loss, including the loss due to Rayleigh scattering and optomechanical coupling, can be extracted from real part of the optical susceptibilities. At zero detuning i.e $\Delta_a = 0$ and $\Delta_b = 0$, the total effective optical loss rates of the $a_\pm$ modes (including waveguide loading) are given by:

$$\kappa_{\text{eff}}^{+} = \kappa\left(1+\mathcal{C}\right)+\frac{4V^2}{\kappa(1+\eta^2\mathcal{C})}, \tag{S7a}$$

$$\kappa_{\text{eff}}^{-} = \kappa(1+\eta^2\mathcal{C})+\frac{4V^2}{\kappa(1+\mathcal{C})}. \tag{S7b}$$

where we define optomechanical cooperativity as $\mathcal{C} = 4G^2/\kappa\Gamma$. If the pump reflection (η) is small, we see that the effective loss rate of the a_+ mode increases with increasing $\mathcal{C}$ in Eq. (S7a), which corresponds to the results of the optomechanically induced transparency [6, 8, 9]. Meanwhile the second term in Eq. (S7b) decreases with increasing $\mathcal{C}$. This analysis reveals that the Rayleigh backscattering contribution is effectively shut down in the limit of large $\mathcal{C}$.

C. Redefining the condition for critical coupling

For conventional resonator-waveguide systems, the transmission through the waveguide in either direction is given by

$$T = \frac{(\kappa-2\kappa_{\text{ex}})/2+i\Delta}{\kappa/2+i\Delta}$$

which can be derived by setting $G \to \infty$ and $V \to 0$ in Eqn. S3a. Critical coupling, the point where on-resonance ($\Delta = 0$) transmission dips to zero in conventional resonator systems is achieved when $\kappa_{\text{ex}} = \kappa/2$. However this condition for achieving critical coupling must be modified in our system. For probing of the ccw optical mode (backward direction), we can rewrite the transmission coefficient at zero detuning ($\Delta_a = 0$ and $\Delta_b = 0$) as described in Eqn. S3b:

$$T_{12} = \frac{\kappa_{\text{eff}}^{-}-2\kappa_{\text{ex}}}{\kappa_{\text{eff}}^{-}} = \frac{\kappa(1+\eta^2\mathcal{C})+4V^2/\kappa(1+\mathcal{C})-2\kappa_{\text{ex}}}{\kappa(1+\eta^2\mathcal{C})+4V^2/\kappa(1+\mathcal{C})} \tag{S8}$$

In other words, the external coupling rate needed to reach critical coupling of the ccw a_- mode with the waveguide should be modified to the following :

$$\kappa_{\text{ex}} = \frac{\kappa_{\text{eff}}^{-}}{2} = \frac{\kappa(1+\eta^2\mathcal{C})}{2}+\frac{2V^2}{\kappa(1+\mathcal{C})} \tag{S9}$$

D. Evolution of transmission and reflection coefficients

In Figure S3 we invoke the model of Eqns. S4 to predict the evolution of transmission and reflection coefficients as a function of optomechanical coupling rate and the optical probe detuning. We have modeled an undercoupled situation, i.e. where the effective intrinsic loss rate of the optical modes is greater than the extrinsic loss under zero optomechanical coupling [10, 11], to correspond with the experiments presented in the main text.

For $G = 0$ the model simply predicts the Rayleigh-scattering induced doublet of the hybridized optical modes. When we engage the unidirectional cw pump (i.e. $G \neq 0$), the forward transmission model T_{21} reveals that a_+ undergoes normal mode splitting caused by optomechanical coupling with the b_+ mechanical mode. Intuitively, we anticipate that the reflection coefficient for the photons in the resonator should be reduced since the lowered photonic susceptibility of the forward subsystem 'open circuits' the reflection pathway mediated by Rayleigh scattering. The reflection coefficient produced by the model agrees with this intuitive assertion. More importantly, the backward transmission coefficient T_{12} shows that the linewidth of the time-reversed mode a_- narrows when G increases, indicating that the intrinsic optical loss rate for that mode is reduced (see §B). A better confirmation of this reduction of intrinsic loss comes from the fact that the a_- mode approaches critical coupling (zero on-resonance transmission, see §C) as the intrinsic loss approaches the extrinsic loss κ_{ex}.

E. Condition for reaching a quantum point

It is also interesting to calculate the effective temperature of the a_- optical mode due to Rayleigh backscattering. We assume $\eta = 0$ for simplifying the equations of motion, and obtain the equations in the Fourier domain:

$$-i\omega\tilde{a}_+ = -\frac{\kappa}{2}\tilde{a}_+ - iG\tilde{b}_+ - iV\tilde{a}_- + \sqrt{\kappa_i}\tilde{a}_{\text{vac}}(\omega) \tag{S10a}$$

$$-i\omega\tilde{b}_+ = -\frac{\Gamma}{2}\tilde{b}_+ - iG^*\tilde{a}_+ + \sqrt{\Gamma}\tilde{b}_{\text{th}}(\omega) \tag{S10b}$$

$$-i\omega\tilde{a}_- = -\frac{\kappa}{2}\tilde{a}_- - iV\tilde{a}_+ + \sqrt{\kappa_i}\tilde{a}_{\text{vac}}(\omega) \tag{S10c}$$

We note that optical noise for the $a_\pm$ modes is negligible due to the negligible thermal excitation of photons. In our system, the additional thermal load on the a_+ mode is $-iG\sqrt{\Gamma}\tilde{b}_{\text{th}}/(\Gamma/2 - i\omega)$ due to the optomechanical interaction. This thermal noise on the a_+ mode excited by the pump is in turn loaded to its degenerate mode a_- through the Rayleigh backscattering channel. Therefore the effective photon occupation of the a_- mode due to the pump in the cw direction becomes:

$$N_{th} = \frac{4\mathcal{C}V^2}{\kappa^2(1+\mathcal{C})^2}n_{th} \tag{S11}$$

where n_{th} is the phonon occupation number at operation temperature, in this case at room temperature. Consequently, quantum optical effects should be observable for very large optomechanical cooperativity, in the regime $\mathcal{C} > 2n_{th}V^2/\kappa^2$.

F. Normal modes without pump backscattering (two-mode split)

The optomechanical hybridization of the optical mode a_+ and mechanical mode b_+ can be seen in either the mechanical or optical spectra. Optical frequency measurement of the normal modes in the strong coupling regime was presented in the main text Fig. 4. These normal modes are also observable through the mechanical spectrum, which is presented through pump scattering measurements [12] in Fig. S4a. To model this system, we chose a frame rotating with the pump laser frequency ω_{pump}, i.e. we re-write $a_+ = a_+ e^{-i\omega_{\text{pump}} t}$, to obtain the mechanical frequency normal modes. As we will show later, the pump backscattering factor η in this experiment is small enough so as to be negligible. We can thus rewrite the equations of motion for the cw modes Eqns. S1 in matrix form as follows:

$$\frac{d}{dt}\begin{bmatrix} a_+ \\ b_+ \end{bmatrix} = -i\begin{bmatrix} -i\frac{\kappa+4V^2/\kappa}{2} + (\omega_a - \omega_{\text{pump}}) & G \\ G^* & -i\frac{\Gamma}{2} + \omega_b \end{bmatrix}\begin{bmatrix} a_+ \\ b_+ \end{bmatrix} \tag{S12}$$

where $\kappa + 4V^2/\kappa$ is the combined optical loss rate including the loss contribution from Rayleigh backscattering into mode a_-. The eigenvalues for the matrix in Eqn. S12 are evaluated as :

$$\lambda_\pm = -i\frac{\kappa+4V^2/\kappa+\Gamma}{4} + \frac{\omega_a+\omega_b-\omega_{\text{pump}}}{2} \pm \frac{1}{2}\sqrt{4G^2 + \left[\Delta^2 + i\left(\frac{\Gamma}{2} - \frac{\kappa+4V^2/\kappa}{2}\right)\right]^2} \tag{S13}$$

Here $\Delta = (\omega_a - \omega_b) - \omega_{\text{pump}}$ is the pump laser detuning that we also define in the main text. We can now obtain the normal mode frequencies by taking the real parts of the eigenvalues in Eqn. S13. Figure S4b compares the experimental data to the theoretical prediction from this analysis. The dots represent the measured peak frequencies for each normal mode in Fig. S4a. The blue and red curves show the theoretical prediction based on Eqn. S13 for the given parameters $G = 0.5$ MHz, $\kappa = 0.62$ MHz, $V = 0.3$ MHz, $\omega_b = 229.6$ MHz and $\Gamma = 39.1$ kHz, which are extracted from Fig. 4 in the main text.

The experimental results presented in Fig. S4 show only two normal-modes in the mechanical domain, corresponding to coupling of the cw a_+ optical mode with the cw b_+ mechanical mode. As we show next, this assures us that there is negligible ccw optomechanical interaction due to backscattering of the pump.

G. Normal modes including pump backscattering (four-mode split)

We can now also examine the corrections to the normal mode splitting that arise if pump backscattering is not negligible. Once again, we use the pump frequency ω_{pump} as reference, and rewrite the more general equations of motion (Eqn. S1) in matrix form.

$$\frac{d}{dt}\begin{bmatrix} a_+ \\ b_+ \\ a_- \\ b_- \end{bmatrix} = -i\begin{bmatrix} -i\frac{\kappa}{2}+\Delta_a & G & V & 0 \\ G^* & -i\frac{\Gamma}{2}+\omega_b & 0 & 0 \\ V & 0 & -i\frac{\kappa}{2}+\Delta_a & -i\eta G \\ 0 & 0 & i\eta G^* & -i\frac{\Gamma}{2}+\omega_b \end{bmatrix}\begin{bmatrix} a_+ \\ b_+ \\ a_- \\ b_- \end{bmatrix} \tag{S14}$$

The coupling terms of the matrix in Eqn. S14 imply that this system will have four normal modes. The spectra of these normal modes can be observed using the mechanical spectrum Fig. S5a. In Fig. S5b we present the analytical eigenvalue curves for the four normal modes based on Eqn. S14, using the parameters $(\kappa, G, V, \omega_b, \eta, \Gamma)$ = (0.6 MHz, 0.4 MHz, 0.85 MHz, 115.03 MHz, 0.7, 10 kHz) that correspond to this experiment. We have specifically avoided such cases in the experiment that we present in the main text, so as to have a clean determination of how cw pump induced time-reversal symmetry breaking affects only the $a_\pm$ modes.

H. Calculation of single photon Brillouin optomechanical coupling

In the previous section, we define the single photon Brillouin optomechanical coupling rate $g_o \propto \delta(\Delta k)\int \phi_1\phi_2\psi\, d^2r$. Here let us describe the quantitative derivation of the optomechanical coupling through an overlap integral. Suppose that the two optical and mechanical modes propagate in the z direction only, so the spatial mode functions for these modes can be written through the method of separation of variables [13].

$$\begin{aligned} \bar{\phi}_1(x,y,z) &= \phi_1(x,y)e^{ik_1 z} \\ \bar{\phi}_2(x,y,z) &= \phi_2(x,y)e^{ik_2 z} \\ \bar{\psi}(x,y,z) &= \psi(x,y)e^{iqz}, \end{aligned} \tag{S15}$$

where k_1, k_2 and q are the momentums of two optical and mechanical modes, respectively. Here the integration of these spatial mode functions represents how strong the coupling of the three modes is. For the forward Brillouin scattering, we already knew the optomechanical interaction $H^{\text{OM}}_{\text{int}} = \hbar(g_o c_+ a_+^\dagger b_+ + g_o^* c_+^\dagger a_+ b_+^\dagger)$ as shown in Fig. S6. Thus the single photon Brillouin optomechanical coupling for the forward scattering is derived by integrating three wavefunctions over space.

$$\begin{aligned} g_o \propto & \iiint dxdydz\bar{\phi}_1(x,y,z)\bar{\phi}_2^*(x,y,z)\bar{\psi}(x,y,z) \\ =& \iiint dxdydz\phi_1(x,y)\phi_2(x,y)\psi(x,y)e^{i(k_1-k_2+q)z} \\ =& \int_{-L/2}^{L/2} dz e^{i\Delta kz} \iint dxdy\phi_1(x,y)\phi_2(x,y)\psi(x,y) \\ =& 2\frac{\sin(\Delta kL/2)}{\Delta k} \iint dxdy\phi_1(x,y)\phi_2(x,y)\psi(x,y), \end{aligned} \tag{S16}$$

where L is the propagation length of the three modes in the z direction. Suppose that these three modes travel in the azimuthal direction, so L must be a perimeter of the resonator. As the momentum difference Δk is much smaller than the perimeter L illustrated in Fig. S6 which is of main interest, we can approximate Eq. (S16). From the relation in the limit of L i.e., $\delta(x) = \lim_{L\to\infty} \sin(xL)/\pi x$, the factor of this overlap integral in Eq. (S16) becomes $2\pi\delta(\Delta k)$ which is identical to our definition of the optomechanical coupling.

2. DETAILS ON EXPERIMENTAL MEASUREMENTS

A. Description of experimental setup

The measurement setup used for our experiments is presented in Fig. S7. We employed fused-silica microsphere resonators, produced on fiber using arc discharge reflow, that are evanescently coupled to a taper fiber waveguide for probing. A 1520 nm to 1570 nm tunable external cavity diode laser was employed to drive optical pump into the waveguide. The laser source was split into the forward and backward pathways using a 90/10 splitter. An Erbium-doped fiber amplifier (EDFA) amplifies the pump power in the forward pathway only (i.e. for cw pumping of the resonator). Electro-optic modulators (EOMs) are used for regulating pump power in both directions by modifying their respective dc bias, and also for producing the optical probes. Fiber polarization controllers (FPC) are used to adjust the forward and backward probe polarizations to match the resonator modes.

During experiments, the probe sidebands generated by the EOMs are swept through the $a_\pm$ mode. The input and output fields are measured at four photodetectors; the optical signals after coupling to the resonator are collected at PD1 and PD2. Alongside, PD3 and PD4 are placed just after the EOMs to obtain 1% of the optical signal for reference. We use two circulators for performing simultaneous measurement of the forward and backward probe transmissions and reflections.

B. Calibration of optical transmission and reflection coefficients

B.1. Transmission coefficients

Here we describe the procedure for determination of transmission coefficients of the probe signals using a network analyzer.

For illustration purposes, the schematic of a typical transmission measurement is presented in Fig. S8a. We use 1 % of the modulated signal after the EOM as a reference at photodetector R, while 99 % of the signal is coupled to the resonator via waveguide and its transmission is measured at photodetector A. Since we use an EOM to produce the probe signal (from the pump), there exist two sidebands $\omega_{\text{pump}} \pm \omega_m$ relative to the pump that propagate through the system, where ω_m is the modulation frequency received from the network analyzer. All optical signals and their positions in frequency space are illustrated in Fig. S8b. Only the upper sideband marked S_{upper} measures the $a_\pm$ mode of interest, while the lower sideband marked S_{lower} passes through the waveguide without interacting with the resonator. Therefore, the upper sideband is used as the optical probe.

The received optical intensities at the two photodetectors can then be expressed as:

$$\left| E_R\, e^{-i\omega_{\text{pump}}t} \left(1 + \frac{\mathcal{B}}{2} e^{-i\omega_m t} + \frac{\mathcal{B}}{2} e^{i\omega_m t}\right) + \text{ c.c} \right|^2 \tag{S17a}$$

$$\left| E_A\, e^{-i\omega_{\text{pump}}t} \left(t_c + t_{us}\frac{\mathcal{B}}{2} e^{-i\omega_m t} + t_{ls}\frac{\mathcal{B}}{2} e^{i\omega_m t}\right) + \text{ c.c} \right|^2 \tag{S17b}$$

where $\mathcal{B}$ is the EOM intensity modulation coefficient, while E_R and E_A are the amplitudes of electric fields in the reference and resonator paths respectively. Here we have defined t_c, t_{us} and t_{ls} as the transmission coefficients of the optical carrier (pump), upper sideband (probe), and lower sideband signals, respectively. The output photocurrent is proportional to the optical intensity expressed in Eqns (S17). However, since the detectors have limited bandwidth in the RF domain, and the network analyzer only measures terms at frequency ω_m, the only terms of interest in the output photocurrents are :

$$R = 2|E_R|^2\mathcal{B}\cos(\omega_m t) \tag{S18a}$$

$$A = \frac{t_c|E_A|^2\mathcal{B}}{2}\left(e^{i\omega_m t} + t_p e^{-i\omega_m(t+\phi')}\right) + \text{ c.c} \tag{S18b}$$

Here, we have simplified $t_c = t_c^*$ to set it as a reference phase, $t_{ls} = e^{i\omega_m\phi'}$ since the lower sideband does not interact with the resonator, and $t_{us} = t_p e^{-i\omega_m\phi'}$ with the new subscript indicating that it is the optical probe. We can now rewrite Eqn. (S18b) as follows :

$$\begin{aligned} A = \frac{t_c|E_A|^2\mathcal{B}}{2} \Big[&\Big\{(1+t_p')\cos(\omega_m\phi') + t_p''\sin(\omega_m\phi')\Big\}\cos(\omega_m t) \\ &+ \Big\{t_p''\cos(\omega_m\phi') - (1+t_p')\sin(\omega_m\phi')\Big\}\sin(\omega_m t)\Big] \end{aligned}$$

The network analyzer in the configuration of Fig. S8a provides a complex-valued ratio of A to R. This result can be separated into in-phase (X) and quadrature (Y) terms as follows:

$$X = \frac{t_c M}{2}\left[(1+t_p')\cos(\omega_m\phi') + t_p''\sin(\omega_m\phi')\right] \tag{S19a}$$

$$Y = \frac{t_c M}{2}\left[t_p''\cos(\omega_m\phi') - (1+t_p')\sin(\omega_m\phi')\right] \tag{S19b}$$

where M is a proportionality constant that includes the power split ratio (1:99), the slight difference in photodetectors' responsivities, and the difference in gain of the two optical paths. We can then write the calibrated probe transmission coefficient t_m as follows :

$$\begin{aligned} t_m &= X + iY \\ &= \frac{t_c M}{2}\left[(1+t_p'+t_p'')\cos(\omega_m\phi') - i(1+t_p'+t_p'')\sin(\omega_m\phi')\right] \\ &= \frac{t_c M}{2}(1+t_p)e^{-i\Phi}\,. \end{aligned} \tag{S20}$$

Since the carrier (pump) transmission t_c, M, and the waveguide dispersion contribution $\Phi = \omega_m\phi'$ are experimentally measurable, we can extract the true transmission coefficient t_p after performing simple calibrations.

B.2. Reflection coefficients

We can now similarly calibrate the optical response to obtain the reflection coefficient using a backward photodetector (via circulator) on the 99 % branch. The measured optical intensity at this backward photodetector is given as :

$$\left| E_A e^{-i\omega_{\text{pump}}t}\left(r_c + r_{us}\frac{\mathcal{B}}{2}e^{-i\omega_m t} + r_{ls}\frac{\mathcal{B}}{2}e^{i\omega_m t}\right) + \text{ c.c} \right|^2 \tag{S21}$$

where r_c, r_{us} and r_{ls} are the reflection coefficients of carrier, upper sideband and lower sideband modes, respectively. Once again, we set the carrier (pump) as the reference $r_c = r_c^*$, and since the lower sideband does not interact with the resonator we can say $r_{ls} = 0$. We can then rewrite the upper sideband reflection coefficient as $r_{us} = r_p e^{-i\omega_m\phi'}$ to indicate the probe reflection coefficient $r_p = (r_p' + ir_p'')$.

$$\begin{aligned} A = \frac{r_c|E_A|^2\mathcal{B}}{2}\Big[&\Big\{r_p'\cos(\omega_m\phi') + r_p''\sin(\omega_m\phi')\Big\}\cos(\omega_m t) \\ &+ \Big\{r_p''\cos(\omega_m\phi') - r_p'\sin(\omega_m\phi')\Big\}\sin(\omega_m t)\Big] \end{aligned}$$

As before, the in-phase (X) and quadrature (Y) terms from the network analyzer can be written.

$$X = \frac{r_c M}{2}\left[r_p'\cos(\omega_m\phi') + r_p''\sin(\omega_m\phi')\right] \tag{S22a}$$

$$Y = \frac{r_c M}{2}\left[r_p''\cos(\omega_m\phi') - r_p'\sin(\omega_m\phi')\right] \tag{S22b}$$

Once again, we can write $r_m = X + iY$ to produce a calibrated reflection coefficient, from which the true reflection coefficient r_p

can be determined once t_c, M, and $\Phi = \omega_m \phi'$ are experimentally measured.

$$\begin{aligned} r_m &= \frac{r_c M}{2}\left[(r'_p + r''_p)\cos(\omega_m \phi') - i(r'_p + r''_p)\sin(\omega_m \phi')\right] \\ &= \frac{t_c M}{2} r_p e^{-i\Phi} \end{aligned} \tag{S23}$$

REFERENCES

1. D. S. Weiss, V. Sandoghdar, J. Hare, V. Lefèvre-Seguin, J.-M. Raimond, and S. Haroche, "Splitting of high-Q Mie modes induced by light backscattering in silica microspheres," Opt. Lett. **20**, 1835–1837 (1995).
2. M. L. Gorodetsky, A. D. Pryamikov, and V. S. Ilchenko, "Rayleigh scattering in high-Q microspheres," J. Opt. Soc. Am. B **17**, 1051–1057 (2000).
3. T. J. Kippenberg, S. M. Spillane, and K. J. Vahala, "Modal coupling in traveling-wave resonators," Opt. Lett. **27**, 1669–1671 (2002).
4. A. B. Matsko and L. Maleki, "Bose-Hubbard hopping due to resonant Rayleigh scattering," Opt. Lett. **42**, 4764–4767 (2017).
5. A. Mazzei, S. Götzinger, L. de S. Menezes, G. Zumofen, O. Benson, and V. Sandoghdar, "Controlled coupling of counterpropagating whispering-gallery modes by a single rayleigh scatterer: A classical problem in a quantum optical light," Phys. Rev. Lett. **99**, 173603 (2007).
6. J. Kim, M. C. Kuzyk, K. Han, H. Wang, and G. Bahl, "Non-reciprocal Brillouin scattering induced transparency," Nat. Phys. **11**, 275–280 (2015).
7. C.-H. Dong, Z. Shen, C.-L. Zou, Y.-L. Zhang, W. Fu, and G.-C. Guo, "Brillouin-scattering-induced transparency and non-reciprocal light storage," Nat. Commun. **6**, 6193 (2015).
8. S. Weis, R. Rivière, S. Deléglise, E. Gavartin, O. Arcizet, A. Schliesser, and T. J. Kippenberg, "Optomechanically induced transparency," Science. **330**, 1520–1523 (2010).
9. A. H. Safavi-Naeini, T. P. M. Alegre, J. Chan, M. Eichenfield, M. Winger, Q. Lin, J. T. Hill, D. E. Chang, and O. Painter, "Electromagnetically induced transparency and slow light with optomechanics," Nature. **472**, 69–73 (2011).
10. M. L. Gorodetsky, A. A. Savchenkov, and V. S. Ilchenko, "Ultimate Q of optical microsphere resonators," Opt. Lett. **21**, 453–455 (1996).
11. A. Yariv, "Universal relations for coupling of optical power between microresonators and dielectric waveguides," Electron. Lett. **36**, 321–322 (2000).
12. G. Bahl, J. Zehnpfennig, M. Tomes, and T. Carmon, "Stimulated optomechanical excitation of surface acoustic waves in a microdevice," Nat. Commun. **2**, 403 (2011).
13. G. S. Agarwal and S. S. Jha, "Multimode phonon cooling via three-wave parametric interactions with optical fields," Phys. Rev. A **88**, 013815 (2013).

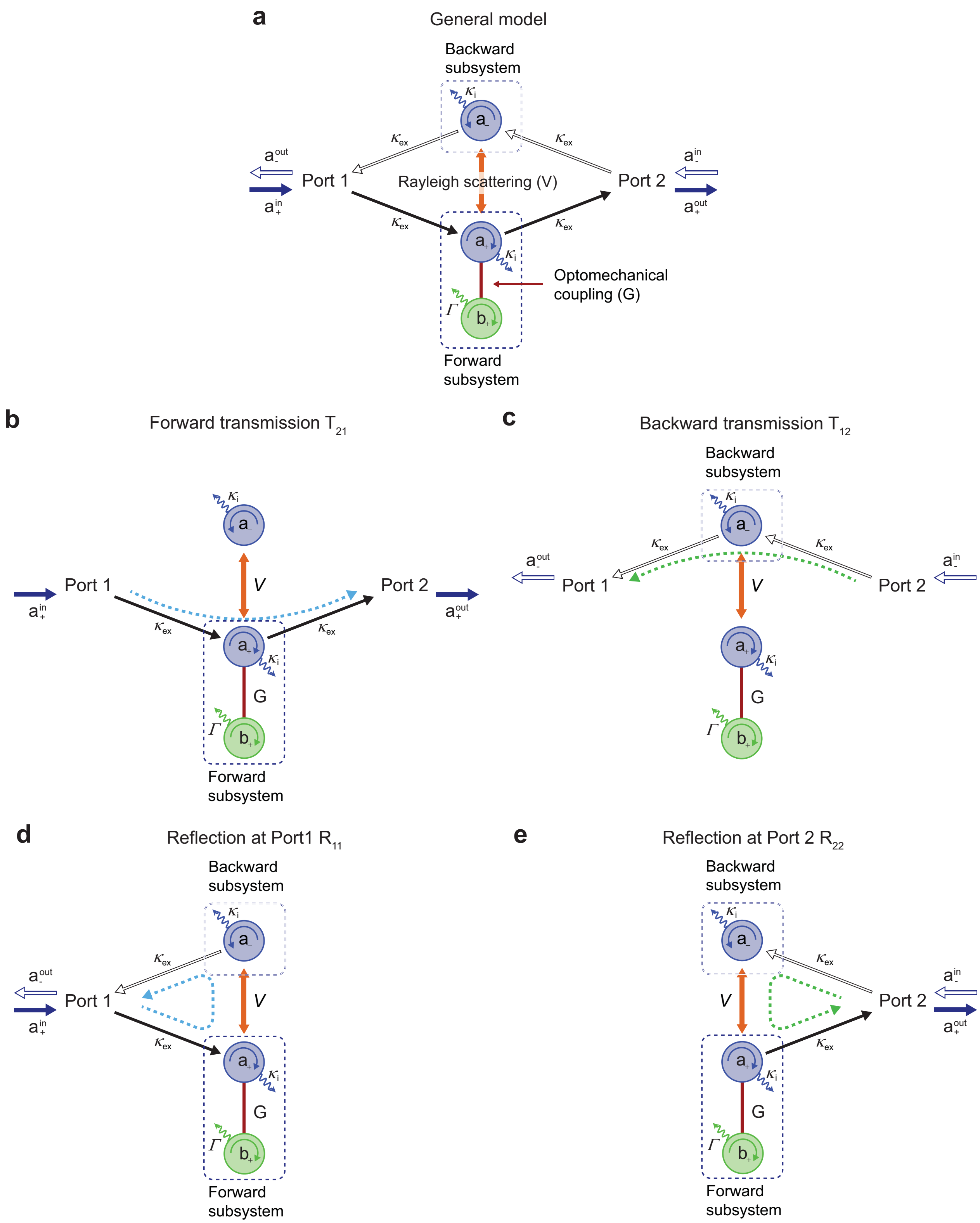

Fig. S1. Toy model for transmission and reflection coefficients. (a) Our system can be described through a two-port system picture, as described in the main manuscript, where each port indicates the left or right ends of the waveguide. Using this, we can describe **(b)** the forward transmission coefficient (T_{21}), **(c)** the backward transmission coefficient (T_{12}), **(d)** the reflection coefficient at Port 1 (R_{11}), and **(e)** the reflection coefficient at Port 2 (R_{22}). The two reflection coefficients R_{11} and R_{22} must be always identical since the interaction takes place through both forward and backward subsystems.

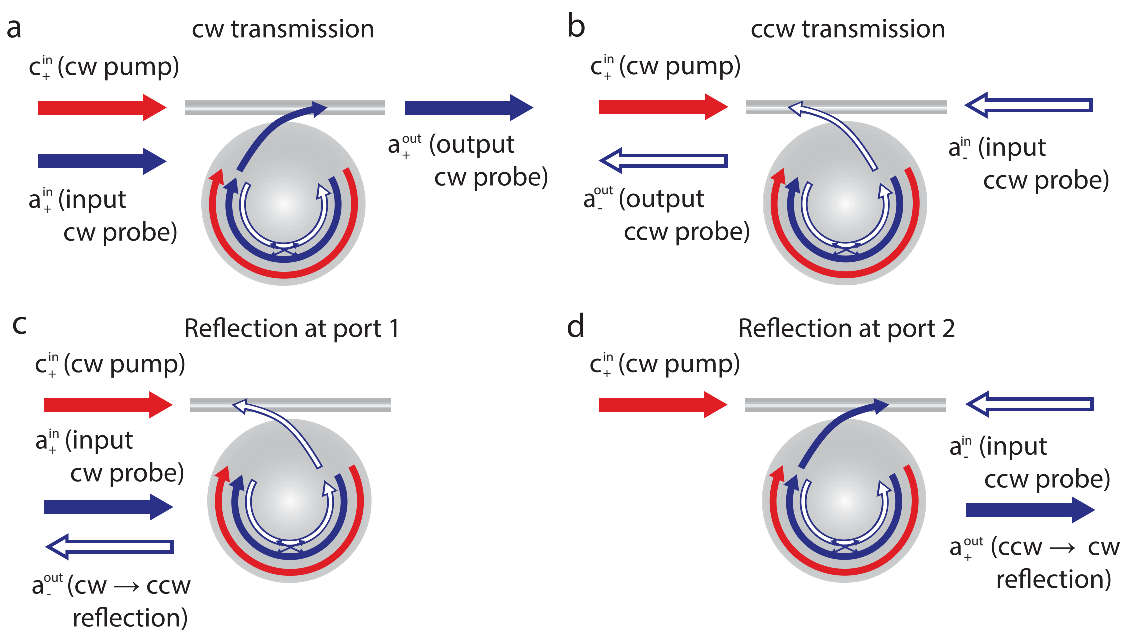

Fig. S2. Variable descriptions for transmission and reflection measurement. For cw optical pumping into the c_+ mode, we can define **(a)** forward transmission, **(b)** backward transmission, **(c)** reflection of the input cw probe a_+^{in} within the probe optical modes $a_\pm$, and **(d)** reflection of the input ccw probe a_-^{in} within the probe optical modes $a_\pm$. As explained in Fig. S1d and S1e the reflections identified in (c) and (d) must be identical.

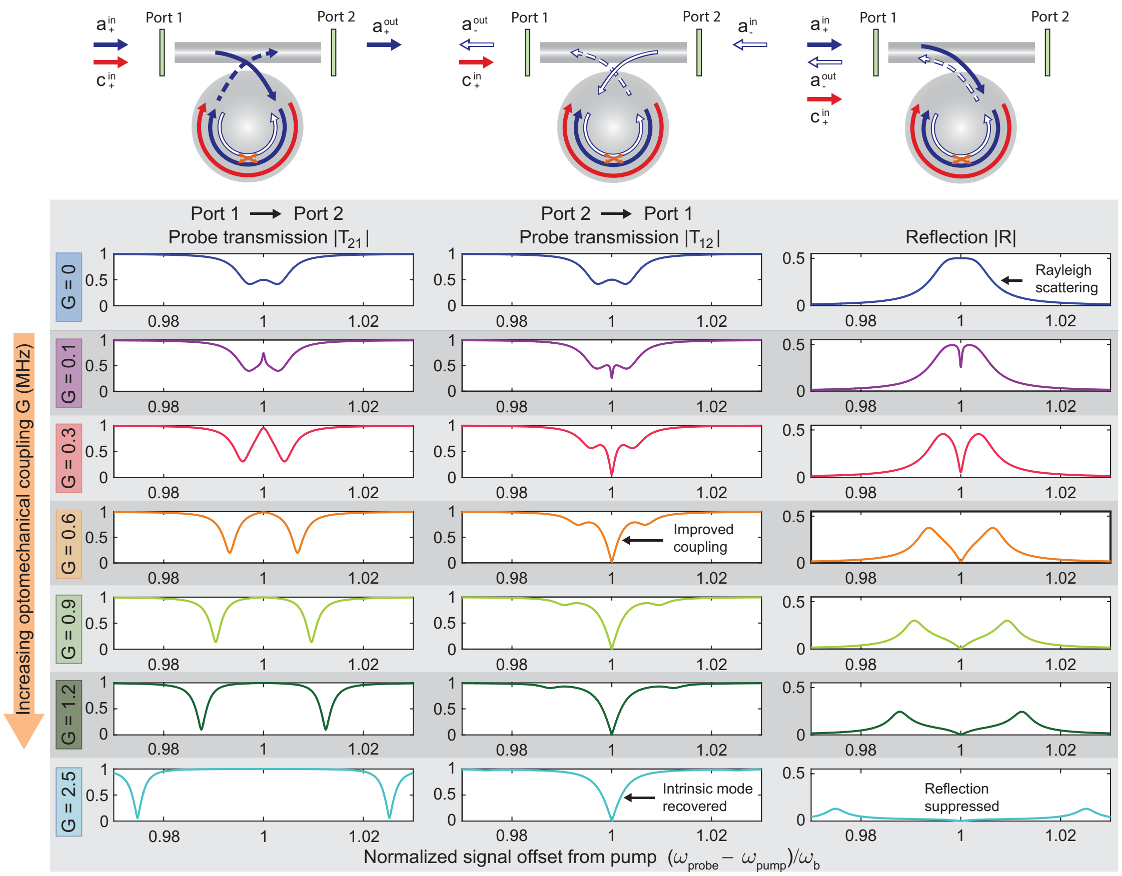

Fig. S3. Theoretical prediction of backscattering suppression. We model the waveguide transmission and reflection coefficients (Eqns. S4) for varying optomechanical coupling rate G. The model parameters are $\kappa = 0.7$ MHz, $\kappa_{\text{ex}} = 0.35$ MHz, $\Gamma = 30$ kHz, and $V = 0.35$ MHz to correspond closely with experiments below. Without any optomechanical coupling ($G = 0$), as is typical, the $a_{\pm}$ modes exhibit the Rayleigh scattering induced doublet and produce identical waveguide transmission coefficients in both directions. Additionally, the resonant Rayleigh backscattering produces a large back-reflection coefficient. Since the effective optical loss for $G = 0$ is $\kappa_{\text{eff}}^{\pm} = \kappa + 4V^2/\kappa = 1.4$ MHz (see Eqns. S7) the system is initially overcoupled at its resonance. However, as G is increased, the time-reversal symmetry of the cw/ccw modes is broken, which can be observed through the strong distinction of transmission coefficients. The resulting suppression of Rayleigh backscattering can be seen in both the reduced reflection coefficient, as well as the improved coupling of the ccw resonator mode in the backward direction (reduced intrinsic loss).

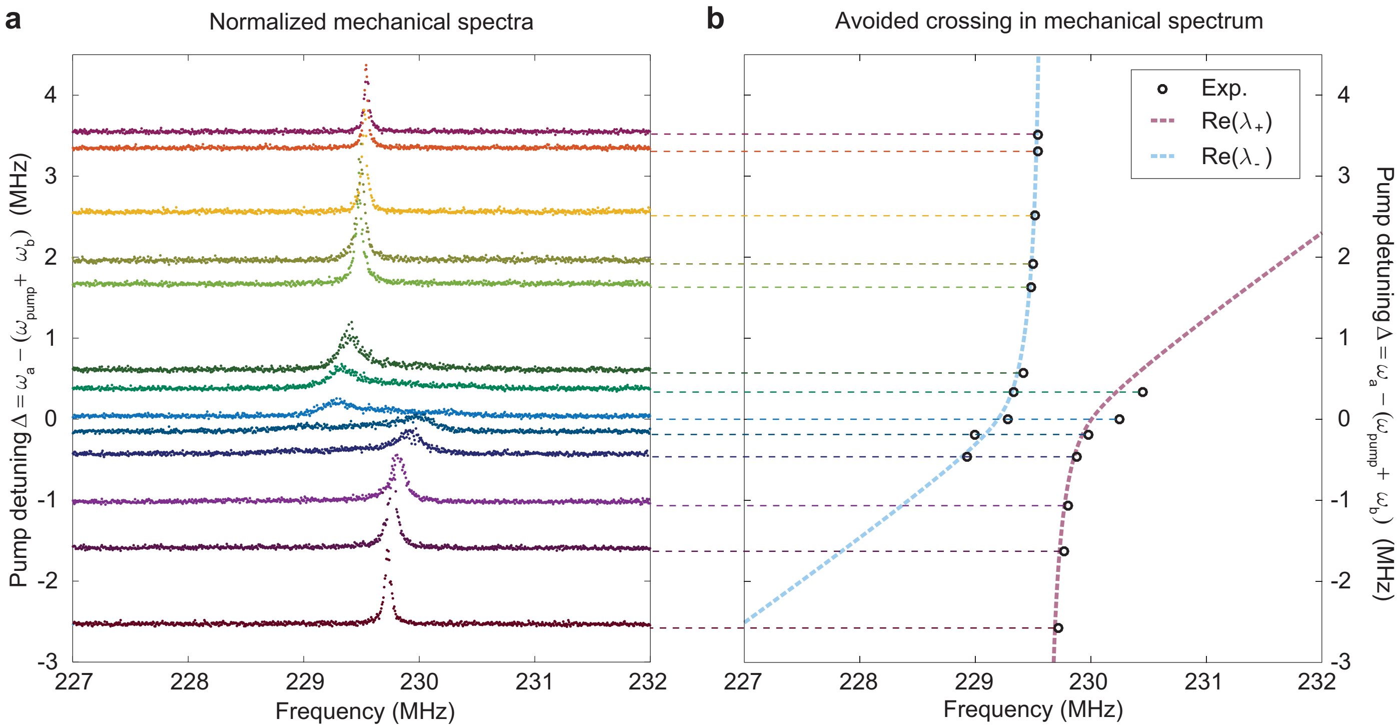

Fig. S4. Normal mode splitting with negligible pump backscattering. (a) We measure the mechanical spectrum through homodyne detection of the beating of the pump and scattered light. The two normal modes resulting from coupling of the a_+ optical and b_+ mechanical modes can be readily seen. This experimental measurement of mechanical spectra corresponds to Fig. 4 in the main text. **(b)** The experimentally measured normal mode frequencies are compared against the theoretical curves of Eqn. S13. Additional details are provided in the text.

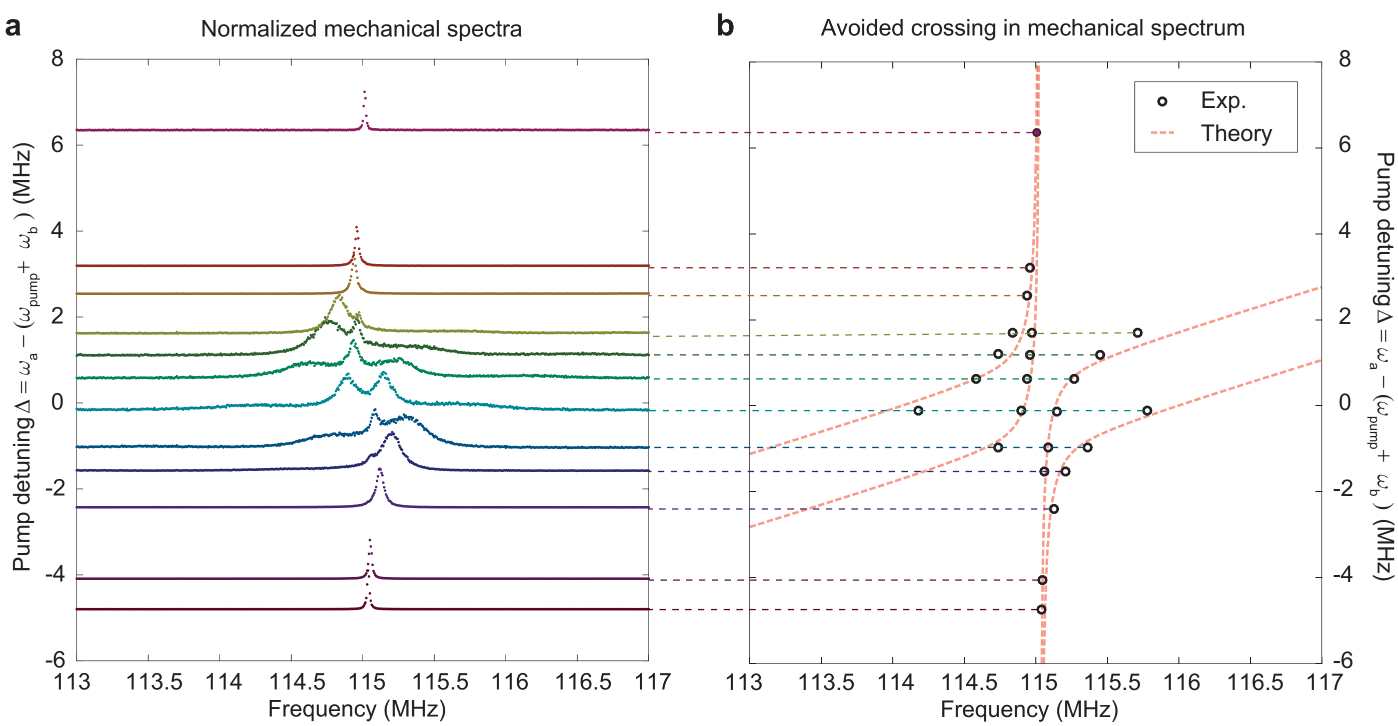

Fig. S5. Normal mode splitting with appreciable pump backscattering. (a) In this case, the mechanical spectra show four normal modes, produced by the optomechanical coupling of $a_\pm$ with their corresponding $b_\pm$, and through the Rayleigh scattering induced coupling of $a_\pm$. **(b)** The experimentally measured normal mode frequencies are compared against the theoretical curves of Eqn. S14. Additional details are provided in the text.

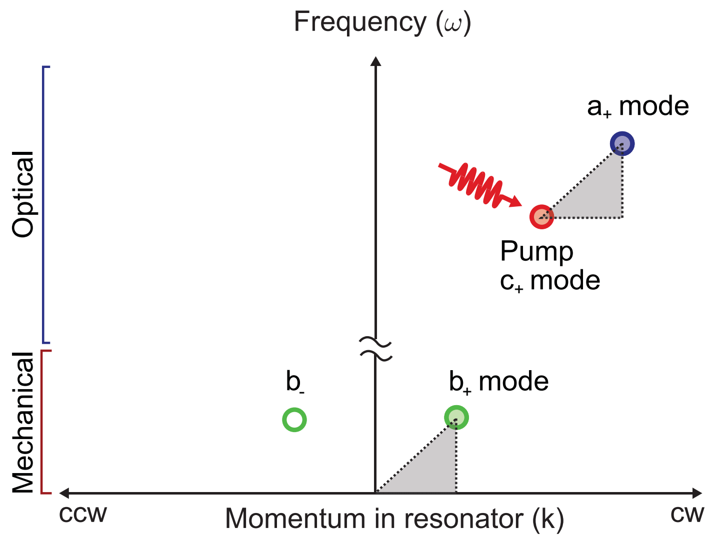

Fig. S6. Illustration of $\omega - k$ diagram for the forward intermodal Brillouin scattering. The two optical modes (a_+ and $b+$) in different families interact with the mechanical mode b_+ through intermodal Brillouin transition. Owing to the phase matching condition, this interaction decays exponentially with varying the momentum difference Δk as described in Eq. (S16).

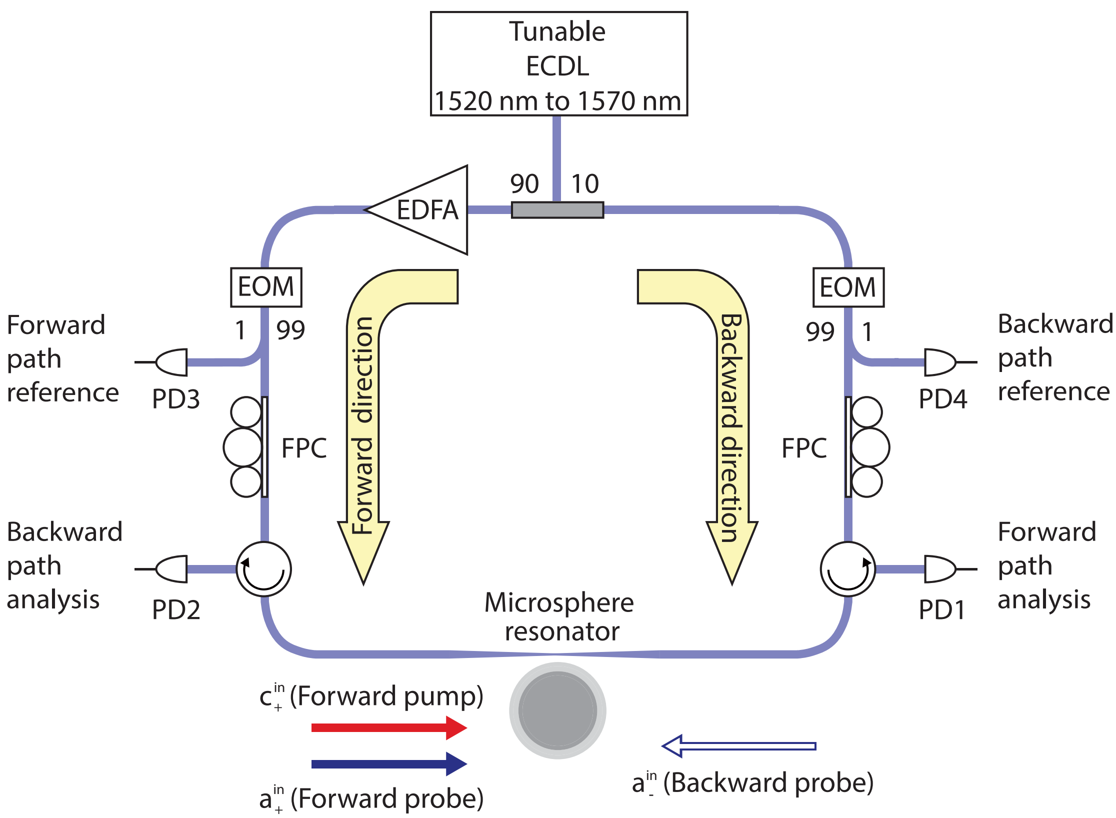

Fig. S7. Experimental setup details. A fiber-coupled tunable external cavity diode laser (ECDL) is sent through a 90/10 fiber splitter to produce forward and backward propagating optical signals. An erbium doped fiber amplifier (EDFA) in the forward direction controls the pump laser power. Electro-optic modulators (EOMs) are additionally help produce the forward and backward probes laser, while fiber polarization controllers (FPCs) are used to match polarization with the resonator modes. Four photodetectors (PDs) help perform transmission and reflection measurements assisted by circulators. The measured signals from the PDs are analyzed using an oscilloscope, electrical spectrum analyzer, and an electrical network analyzer.

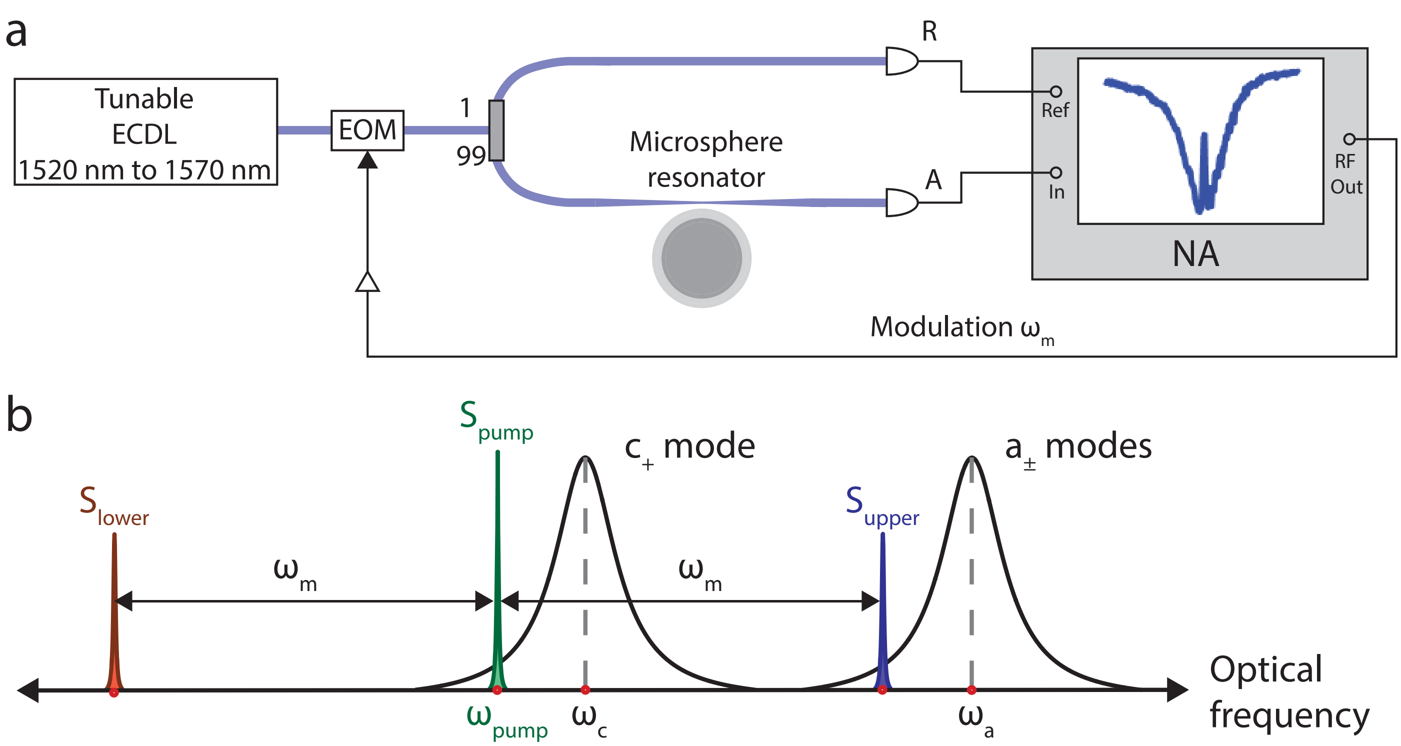

Fig. S8. **(a)** Schematic for transmission measurements distilled from Fig. S7. **(b)** The EOM produces two optical sidebands to the pump or carrier laser field (S_{pump}). While the pump is parked within the c_+ mode, the upper sideband is able to probe the $a_\pm$ modes. We detail the mathematics for the measurement in §B.1.